

Tunable quantum switcher and router of cold atom matter waves using artificial magnetic fields

Yan-Jun Zhao,¹ Dongyang Yu,² Boyang Liu,³ and Wu-Ming Liu^{2,4}

¹*Faculty of Information Technology, College of Microelectronics,
Beijing University of Technology, Beijing, 100124, People's Republic of China*

²*Beijing National Laboratory for Condensed Matter Physics,
Institute of Physics, Chinese Academy of Sciences, Beijing 100190, China*

³*Institute of Theoretical Physics, Beijing University of Technology, Beijing 100124, China*

⁴*School of Physical Sciences, University of Chinese Academy of Sciences, Beijing 100190, China*
(Revised July 23, 2019)

We investigate the single-atom transport in a two-leg ladder with only two rungs, which together with the legs, enclose an artificial magnetic flux. Here, the atoms on the two legs possess opposite onsite energies that produce an energy offset. We find that the atom incoming from the left leg can experience from blockade to transparency via modifying the onsite energy, hopping strength, or magnetic flux, which can be potentially used for a quantum switcher. Furthermore, the atom incoming from the left leg can also be perfectly routed into the right leg, when, intriguingly, the outgoing atom in the R channel possesses a wavevector that can be modulated by the magnetic flux. The result may be potentially used for the interface that controls the communication between two individual quantum devices of cold atoms. The method can also be generalized to other artificial quantum systems, such as superconducting quantum circuit system, optomechanical system, etc.

PACS numbers: 37.10.Jk, 03.75.Lm, 05.45. a, 05.60.Gg, 42.25.Bs

I. INTRODUCTION

The artificial tunability has made ultracold atoms an attractive platform for conducting research on quantum information processing [1–4] and high-precision instruments [5–9]. Integrating different cold atom systems together, one can possibly realize the scalable quantum network, with each quantum node being a cold atom subsystem. However, reaching this destination demands the coherent manipulation of cold atom matter waves such that different nodes can be individually addressed for the effective communication of quantum signals. To this end, there have already been many researches on matter wave transport based on atom interactions [10–25]. For example, matter wave switchers have been proposed for spinless [10] and spinful [11] plane waves. Besides, spinful plane waves with opposite spins can also be isolated and converted [11]. However, both schemes [10, 11] rely on first preparation of a localized Bose-Einstein condensate (BEC), which increases the complexity in experiment. Moreover, to practically control the signal flow in quantum network, the ideal quantum router needs to have multiaccess channels, which has been studied in the circuit QED system [26] but rarely investigated in cold atom systems.

Meanwhile, we have noted that chiral currents can emerge in bosonic ladders due to the effect of the artificial magnetic field [27]. This motivates us to explore the quantum switcher and router controlled by the artificial magnetic field which can coherently couple two individual atomic channels together. In detail, we consider that the magnetic flux only penetrates one particular loop enclosed by four lattice sites, while elsewhere, the two legs of the ladders are decoupled but lifted by an energy detuning. We will study the transport properties in the single-atom scenario for the incident plane wave with varying energy detunings and magnetic fluxes. We will demonstrate that the one-channel switcher and two-channel router can be

realized within our model.

Our paper is organized as follows. In Sec. II, we introduce the Hamiltonian and derive the single-atom scattering coefficients between the two atomic channels. In Sec. III, we discuss the single-atom switcher effect for different parameters. In Sec. IV, we demonstrate that the model can also be used as single-atom router. In Sec. V, we make some discussions in experiment and conclude the main results.

II. SINGLE-ATOM TRANSPORT

A. Two-channel interaction

We study the scattering problem for a single-atom plane wave from the L leg of the bosonic ladders incident on a loop enclosing an artificial magnetic flux ϕ (see Fig. 1). The L and R legs, detuned by onsite energies $\varepsilon_L = \varepsilon$ and $\varepsilon_R = -\varepsilon$, are decoupled except at the sites on the loop [see Appendix. A for details of the experimental realization]. Away from the loop, the reflection and transmission will be stimulated. The intra-leg hopping strengths are respectively J_L and J_R for the L and R legs. The interleg hopping strengths are K and $K \exp(i\phi)$ for the sites $l = 0$ and $l = 1$. The theoretical model can be characterized by the following Hamiltonian

$$\begin{aligned}
 H = & \sum_l \varepsilon_R b_{l,R}^\dagger b_{l,R} + \varepsilon_L b_{l,L}^\dagger b_{l,L} \\
 & - \sum_l (J_R b_{l+1,R}^\dagger b_{l,R} + J_L b_{l+1,L}^\dagger b_{l,L}) + \text{H.c.} \\
 & - K b_{0,L}^\dagger b_{0,R} - K e^{-i\phi} b_{1,L}^\dagger b_{1,R} + \text{H.c.}, \quad (1)
 \end{aligned}$$

where $b_{l,\sigma}$ and $b_{l,\sigma}^\dagger$ ($\sigma = L, R$) are the bosonic annihilation and creation operators for the σ leg at site l .

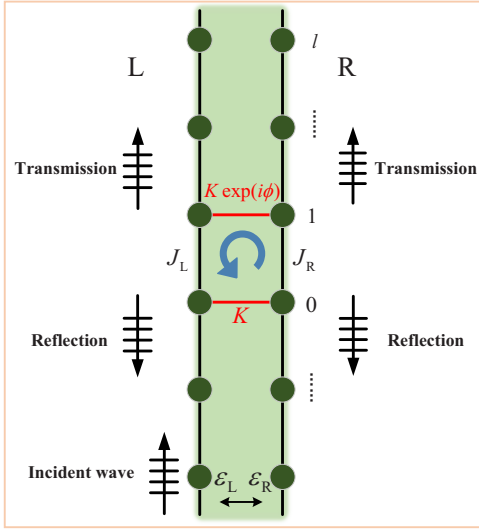


FIG. 1: (color online). Scattering process of a single-atom plane wave along the L leg of the ladder model running into the loop penetrated by a artificial magnetic flux ϕ . The L and R legs are decoupled except at the very four sites at $l = 0$ and $l = 1$ that encloses the magnetic flux. Away from the loop, the reflection and transmission will be stimulated in both channels. The intraleg hopping strengths are respectively J_L and J_R for the L and R legs. The interleg hopping strengths are respectively K and $K \exp(i\phi)$ for the site $l = 0$ and $l = 1$. The onsite energies for the L and R legs are respectively $\varepsilon_L = \varepsilon$ and $\varepsilon_R = -\varepsilon$.

The single-atom eigenstate of the full Hamiltonian can be given by $|E\rangle = \sum_l u_{l,R} b_{l,R}^\dagger |0\rangle + u_{l,L} b_{l,L}^\dagger |0\rangle$, where the coefficients $u_{l,\mu}$ for each single-atom component are constrained by

$$E u_{l,R} = \varepsilon_R u_{l,R} - J_R (u_{l-1,R} + u_{l+1,R}) - \delta_{l,0} K u_{l,L} - \delta_{l,1} K e^{i\phi} u_{l,L}, \quad (2)$$

$$E u_{l,L} = \varepsilon_L u_{l,L} - J_L (u_{l-1,L} + u_{l+1,L}) - \delta_{l,0} K u_{l,R} - \delta_{l,1} K e^{-i\phi} u_{l,R}. \quad (3)$$

One can see that the interaction between both channels are determined by the coupling strength K and magnetic flux ϕ at $l = 0, 1$.

B. Free modes

Now, assuming the interaction between both channels is zero, i.e., setting $K = 0$ in Eqs. (2) and (3), we can obtain the free modes in both channels as

$$u_{l,\sigma} = e^{ik_\sigma l}, \quad (4)$$

where the energy E depends on k_σ according to the relation

$$E = \varepsilon_\sigma - 2J_\sigma \cos k_\sigma. \quad (5)$$

Here, we stress that k_σ can be either real or complex depending on the regime of E . In detail, for either atomic channel $\sigma = L$ or R , the free modes can be classified into three cases:

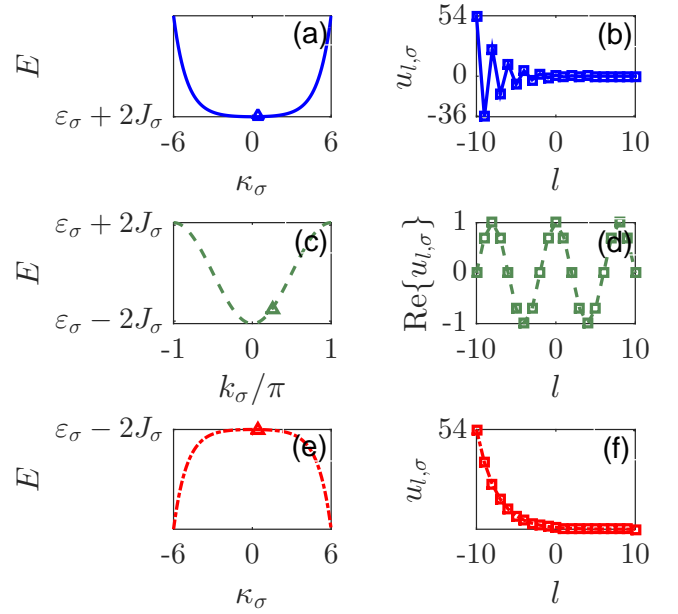


FIG. 2: (color online). Energy and eigenstates: (a) Eigen energy $E_\sigma = \varepsilon_\sigma + 2J_\sigma \cosh \kappa_\sigma$ against κ_σ ($\sigma = L, R$). (b) Eigenstate $u_{l,\sigma} = (-1)^l e^{-\kappa_\sigma l}$ against the lattice site l at $\kappa_\sigma = 0.4$ [Marked by “ Δ ” in (a)]. (c) Eigen energy $E = \varepsilon_\sigma - 2J_\sigma \cos k_\sigma$ against the wave vector k_σ . (d) Real part of the eigenstate $u_{l,\sigma} = e^{ik_\sigma l}$ against l at $k_\sigma = \frac{\pi}{4}$ [Marked by “ Δ ” in (c)]. (e) Eigen energy $E_\sigma = \varepsilon_\sigma - 2J_\sigma \cosh \kappa_\sigma$ against κ_σ . (f) Eigenstate $u_{l,\sigma} = e^{-\kappa_\sigma l}$ against l at $\kappa_\sigma = 0.4$ [Marked by “ Δ ” in (e)].

(i) The energy E belongs to the band $[\varepsilon_\sigma + 2J_\sigma, \infty)$, such that k_σ must be complex and can be rewritten as $k_\sigma = \pi + i\kappa_\sigma$ for real κ_σ . In this case, the energy turns into a hyperbolic cosine, $E = \varepsilon_\sigma + 2J_\sigma \cosh \kappa_\sigma$ [see Fig. 2(a)], and the eigenstate becomes $u_{l,\sigma} = (-1)^l e^{-\kappa_\sigma l}$, a staggered decaying mode [see Fig. 2(b)].

(ii) The energy E is in the band $(\varepsilon_\sigma - 2J_\sigma, \varepsilon_\sigma + 2J_\sigma)$, such that k_σ is guaranteed to be real. In this case, the eigenstate and corresponding energy will retain their original forms as in Eqs. (4) and (5). Dispersive as $E = \varepsilon_\sigma - 2J_\sigma \cos k_\sigma$ [see Fig. 2(c)], the eigenstate $u_{l,\sigma} = e^{ik_\sigma l}$ is a transmission mode [see Fig. 2(d)] with the group velocity $v_g = 2J_\sigma \sin k_\sigma$.

(iii) The energy E belongs to the band $(-\infty, \varepsilon_\sigma - 2J_\sigma)$, such that k is purely imaginary and can be rewritten as $k_\sigma = i\kappa_\sigma$ for real κ . In this case, the energy also turns into a hyperbolic cosine, $E = \varepsilon_\sigma - 2J_\sigma \cosh \kappa_\sigma$ [see Fig. 2(e)], and the eigenstate becomes $u_{l,\sigma} = e^{-\kappa_\sigma l}$, also a decaying mode [see Fig. 2(f)].

C. Single-atom transport

We consider the single-atom plane wave comes from the negative lattices along the L channel, which will be scattered into both L and R channels. In detail, we can express $u_{l,R}$ and

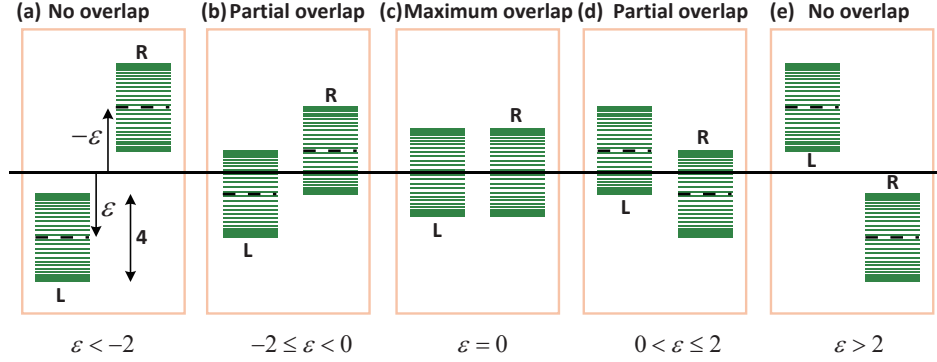


FIG. 3: (color online). Matching relations between transmission energy bands of channels L and R as the detuning ε changes. Here, for simplicity, we have assumed $J_L = J_R = 1$ such that the widths of transmission energy bands are $2J_L = 2J_R = 2$. If (a) $\varepsilon < -2$ or (e) $\varepsilon > 2$, there is no overlap between two transmission bands. However, if (b) $-2 < \varepsilon < 0$ or (d) $0 < \varepsilon < 2$, there is partial overlap. Furthermore, if (c) $\varepsilon = 0$, maximum overlap between two bands emerges.

$u_{l,L}$ as

$$u_{l,L} = (e^{ik_L l} + r_{LL} e^{-ik_L l}) \theta_{-l} + t_{LL} e^{ik_L l} \theta_{l-1}, \quad (6)$$

$$u_{l,R} = r_{RL} e^{-ik_R l} \theta_{-l} + t_{RL} \theta_{l-1}, \quad (7)$$

where θ_l is the Heaviside step function, t_{LL} (r_{LL}) is the transmitted (reflected) amplitude, and t_{RL} (r_{RL}) is the forward (backward) transfer amplitude.

Then, solving Eqs. (2) and (3) by assigning $l = 0, 1$, we finally obtain the scattering coefficients as

$$t_{LL} = D^{-1} (2i \sin k_L) [2i \sin k_R - \xi e^{i(k_R - \phi)}] \quad (8)$$

$$t_{RL} = \frac{K}{J_R} D^{-1} (-2i \sin k_L) [1 + e^{i(k_L - k_R + \phi)}] \quad (9)$$

$$r_{LL} = \xi D^{-1} e^{ik_L} [(2 \cos \phi - \xi) e^{ik_R} + 2 \cos k_L] \quad (10)$$

$$r_{RL} = \frac{K}{J_R} D^{-1} (-2i \sin k_L) [1 + (e^{i\phi} - \xi) e^{i(k_L + k_R)}] \quad (11)$$

where $\xi = \frac{K^2}{J_L J_R}$ represents the normalized square interleg coupling strength and the denominator D reads

$$D = [2i \sin k_L - \xi e^{i(k_L + \phi)}][2i \sin k_R - \xi e^{i(k_R - \phi)}] - \xi [1 + e^{-i(k_L - k_R + \phi)}][1 + e^{i(k_L - k_R + \phi)}]. \quad (12)$$

For the lattice site $l \neq 0, 1$ in Eqs. (2) and (3), we can obtain the energy matching condition

$$E = \varepsilon_L - 2J_L \cos k_L = \varepsilon_R - 2J_R \cos k_R, \quad (13)$$

which renders the constraint of k_L and k_R in Eqs. (8)-(11). Noting that $\varepsilon_L = \varepsilon$ and $\varepsilon_R = -\varepsilon$ have been previously hypothesized as treating Eq. (13), we can then determine that the transmission bands of both channels can have no overlap, partial overlap, or maximum overlap if $|\varepsilon| > J_L + J_R$, $0 < |\varepsilon| < J_L + J_R$, or $\varepsilon = 0$, respectively. Figure 3 has shown the relative position of the transmission energy bands of both channels in the special case $J_L = J_R = 1$ for different ε . In the case of no overlap [see Figs. (a) and (e)], the incoming atom will stimulate a localized profile [$k_R = i\kappa_R$ or $k_R = i\kappa_R + \pi$

with $\kappa_R > 0$, see Eq. (2)], meaning no scattered atom in the R channel. In the case of maximum overlap [see Fig. (c)], the atom incoming from the L channel can be redirected into the R channel (k_R is real). However, in the case of partial overlap [see Figs. (b) and (d)], the atom can either be redirected into the R channel or stimulate a localized profile there, just depending on the detailed energy E for the incoming atom.

III. SWITCHING SINGLE ATOM

Now we explore the possibility to realize the atom switcher in the L channel, a device which can tune the blockade and transparency of the incident atom. The blockade and transparency require that no scattered atom occur in the R channel, where a localized mode should be stimulated instead [$k_R = i\kappa_R$ or $k_R = i\kappa_R + \pi$].

In detail, by investigating Eqs. (8) and (10), we can obtain the condition for blockade ($t_{LL} = 0$, $|r_{LL}| = 1$) as

$$\phi = \pi \quad (14)$$

$$e^{-ik_R} \mp \sqrt{\xi + 1} = 0, \quad (15)$$

$$J_L \cos k_L \mp \frac{J_R}{2} \left(\sqrt{\xi + 1} + \frac{1}{\sqrt{\xi + 1}} \right) - \varepsilon = 0. \quad (16)$$

Similarly, the condition for transparency ($|t_{LL}| = 1$, $|r_{LL}| = 0$) can also be obtained as

$$J_L \cos k_L - \frac{J_R}{2} \left(\frac{2 \cos k_L}{\gamma} + \frac{\gamma}{2 \cos k_L} \right) - \varepsilon = 0, \quad (17)$$

$$e^{ik_R} - \frac{2 \cos k_L}{\gamma} = 0, \quad (18)$$

where $\gamma = \xi - 2 \cos \phi \geq -2$ represents the resultant effect from both ϕ and ξ and $\left| \frac{2 \cos k_L}{\gamma} \right| < 1$ must be satisfied to guarantee that k_R corresponds to a localized mode near the loop: $\exp(ik_R) = \pm \exp(-\kappa_R)$ with $\kappa_R > 0$.

In the special case with equal intraleg hopping strengths: $J_L = J_R = 1$, which results in $\xi = K^2$, the relation in

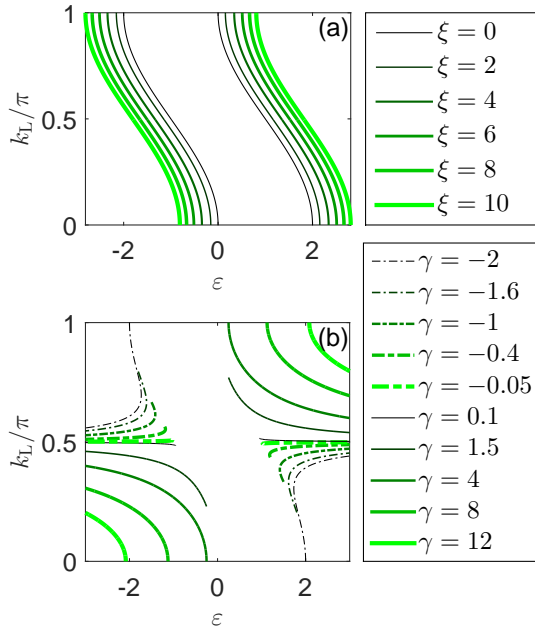


FIG. 4: (color online). Wave vector k_L at (a) blockade [or (b) transparency] point depending on the onsite energy ε for different $\xi = \frac{K^2}{J_L J_R}$ (or $\gamma = \xi - 2 \cos \phi$) in the special case with $J_L = J_R = 1$. The values of ξ and γ are distinguished by both the color, thickness, and line style. Here, J_L (J_R) is the intraleg hopping strength for the L (R) leg, while K the interleg hopping strength. Besides, ϕ is the artificial magnetic flux.

Eqs. (16) and (17) can be illustrated in Fig. 4. We find in Fig. 4(a) that, to blockade the incoming atom at a particular wavevector k_L , one can use a smaller ε in combination with a bigger ξ , or vice versa. For given ξ , the blockade point k_L monotonically decreases as ε increases. In Fig. 4(b), we also see that, if γ is given (e.g., $\gamma = -1.6$, etc), two transparency points may occur if ε is assigned appropriately. The detailed conditions to obtain two transparency points can be obtained as $-2 < \gamma < 0$ and $\sqrt{1-\gamma} < |\varepsilon| \leq 1 - \frac{\gamma}{2}$. Both Fig. 4(a) and Fig. 4(b) are centrally symmetric about ($\varepsilon = 0, k_L = \frac{\pi}{2}$). In addition, $\varepsilon \neq 0$ can be verified, indicating the matching relations of the transmission energy bands correspond to all the subfigures in Fig. 3 except Fig. 3(c). In a word, the transparency and blockade points can be tuned in principle through modifying ϕ , ε , or ξ .

To furthermore gain an intuitive picture, in Fig. 5, we have plotted the transmittance $T_{LL} = |t_{LL}|^2$, reflectance $R_{LL} = |r_{LL}|^2$, and forward (backward) transfer rate $T_{RL} = |t_{RL}|^2$ ($R_{RL} = |r_{RL}|^2$) as the function of k_L for the detailed parameters $\phi = \pi$, $\xi = K^2 = 4$, and different ε . In such parameter setup, the matching relations of the transmission energy bands for both channels are respectively no overlap [$\varepsilon = -2.02$, see Fig. 3(a)], partial overlap [$\varepsilon = -0.7$, see Fig. 3(b)], maximum overlap [$\varepsilon = 0$, see Fig. 3(c)], partial overlap [$\varepsilon = 0.7$, see Fig. 3(d)], and no overlap [$\varepsilon = 2.02$, see Fig. 3(e)] for each column in Fig. 5 from left to right. From the curves of T_{LL} and R_{LL} in Figs. 5(a), 5(c), 5(g), and 5(i), the transparency-

blockade transitions are observed as k_L gradually increases.

In Figs. 5(b), 5(d), 5(h), and 5(j), we also note that the transfer rate T_{RL} can exceed 1. On one hand, this is because T_{RL} and \tilde{T}_{RL} reveal the amplitudes of the localized mode stimulated in R channel when k_R is complex. On the other, if k_R is real, when transmission modes are stimulated in R channel, the atom flow conservation are subject to the relation

$$\tilde{T}_{LL} + \tilde{R}_{LL} + \tilde{T}_{RL} + \tilde{R}_{RL} = 1. \quad (19)$$

Here, $\tilde{T}_{LL} = T_{LL}$ ($\tilde{T}_{RL} = T_{RL} J_R \sin k_R / J_L \sin k_L$) and $\tilde{R}_{LL} = R_{LL}$ ($\tilde{R}_{RL} = R_{RL} J_R \sin k_R / J_L \sin k_L$) are respectively the forward and backward atom flows scattered in the L (R) channel. In this case, one can conclude that T_{RL} can be greater than 1 once k_R is small enough, which features a sufficiently small group velocity ($= J_R \sin k_R$) in R channel. Similarly, R_{RL} can in principle exceed 1 as well. When $\varepsilon = 0$, the equal intraleg hopping strengths $J_L = J_R = 1$ result in $k_R = k_L$, only transmission modes stimulated in R channel. Thus, we have $T_{LL} + R_{LL} + T_{RL} + R_{RL} = 1$, in which case, $T_{LL,RL} < 1$ and $R_{LL,RL} < 1$ always hold [see Figs. 5(e) and 5(f)]. In particular, one finds that $T_{RL} = 0$, which can be verified by Eq. (9) under the condition $k_R = k_L$ and $\phi = \pi$.

Now we investigate the transmittance T_{LL} and reflectance R_{LL} via independently modifying the values of ε , ξ , and ϕ [see Fig. 6]. We see two (one), one (one), and one (two) blockade (transparency) points in Fig. 6(a), 6(b), and 6(c), respectively as ε , ξ , and ϕ varies. The number of blockade or transparency points for ε , ξ , or ϕ can be exactly predicted using Eqs. (14)-(18) with other parameters determined. We also find that the transfer rates T_{RL} and R_{RL} can exceed 1, the reason for which is similar to Fig. 5. Thus, to tune the transport of the atom at a given wavevector, we can optionally select ε , ξ , or ϕ as the controllable parameter.

IV. ROUTING SINGLE ATOM

Now we investigate the phenomenon of routing the atom from the L channel into the R one, in which case, the wavevectors k_L and k_R are both real and thus $|\varepsilon| \leq 2$ must hold [see Figs. 3(b)-3(d)]. Via examining Eqs. (8) and (11), we find that when the normalized square interleg coupling strength ξ and onsite energy ε satisfy the conditions

$$\xi = 2 \cos \phi, \quad (20)$$

$$\varepsilon = J_R \sin \phi, \quad (21)$$

the perfect routing defined by $\tilde{T}_{LL} = \tilde{R}_{LL} = 0$ will occur at

$$k_R = \phi + \frac{\pi}{2}, \quad (22)$$

$$k_L = \frac{\pi}{2}. \quad (23)$$

Here, to guarantee that both ξ and the group velocity corresponding to k_R (i.e., $J_R \sin k_R$) are positive, there should be the constraint $-\frac{\pi}{2} \leq \phi \leq \frac{\pi}{2}$. Under the conditions in Eqs. (20)-(23), the transfer amplitudes are $t_{RL} = r_{RL} =$

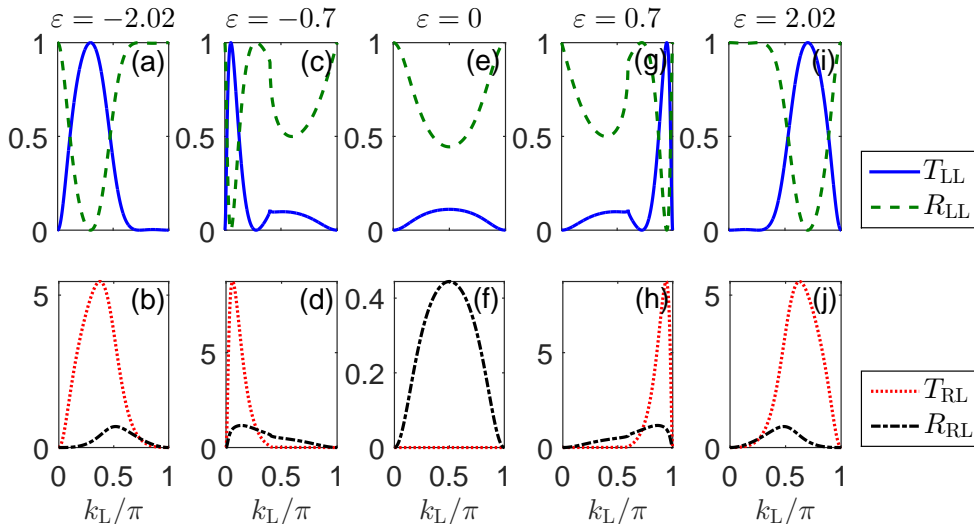


FIG. 5: (color online). Transmittance T_{LL} , reflectance R_{LL} , forward transfer rate T_{RL} , and backward transfer rate R_{RL} against the wave vector k_L (a) and (b). Here, the artificial magnetic flux $\phi = \pi$, the intraleg hopping strengths $J_L = J_R = 1$, and the interleg hopping strength $K = 2$. The onsite energy: (a) and (b) $\varepsilon = -2.02$; (c) and (d) $\varepsilon = -0.7$; (e) and (f) $\varepsilon = 0$; (g) and (h) $\varepsilon = 0.7$; and (i) and (j) $\varepsilon = 2.02$. In such parameter setup, the matching relations of the transmission energy bands of both channels: (a) and (b) no overlap [see Fig. 3(a)]; (c) and (d) partial overlap [see Fig. 3(b)]; (e) and (f) maximum overlap [see Fig. 3(c)]; (g) and (h) partial overlap [see Fig. 3(d)]; (i) and (j) no overlap [see Fig. 3(e)].

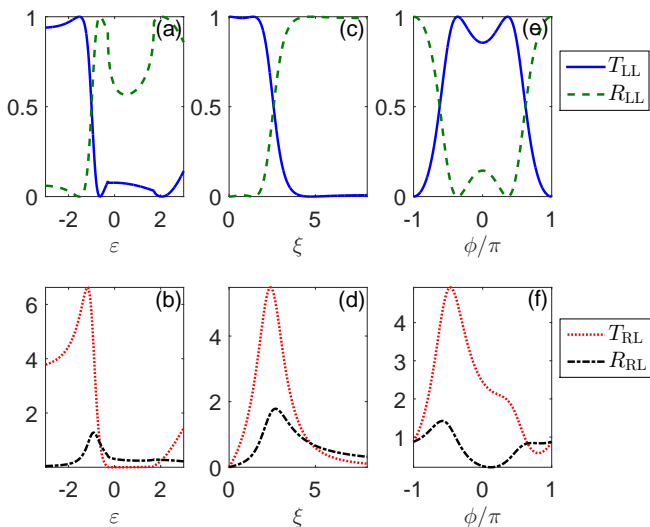


FIG. 6: (color online). Transmittance T_{LL} and reflectance R_{LL} , forward transfer rate T_{RL} , and backward transfer rate R_{RL} depending on the (a) onsite energy ε , (b) normalized square interleg coupling strength $\xi = \frac{K^2}{J_L J_R}$, or (c) artificial magnetic flux ϕ/π . Here, K is the interleg coupling strength. In all plots (a)-(c), we have chosen intraleg hopping strengths $J_L = J_R = 1$ (making $\xi = K^2$) and the wave vector at which the atom incomes $k_L = \frac{\pi}{4}$. In (a) and (b), we set $\phi = \pi$, and $K = 2$ (making $\xi = 4$). In (c) and (d), $\phi = \pi$, and $\varepsilon = -0.7$. In (e) and (f), $K = 2$ (making $\xi = 4$), and ε is assigned according to the blockade condition [see Eq. (16)], i.e., $\varepsilon = -0.6345$.

$\frac{K}{J_R} \frac{i}{2 \cos \phi}$, and the corresponding atom flows are $\tilde{T}_{RL} = \tilde{R}_{RL} = \frac{1}{2}$.

Hereafter, we still consider equal intraleg hopping strengths, i.e., $J_L = J_R = 1$. Figures 7(a)-7(c) have shown respectively how ξ , ε , and k_R at perfect routing [see Eqs. (20)-(22)] will change as ϕ varies from $-\frac{\pi}{2}$ to $\frac{\pi}{2}$. The perfect routing requires that both ξ and ε be sine functions of the artificial magnetic flux ϕ . Besides, the wavevector of the atom outgoing from the R channel can be linearly modulated by ϕ , despite the fact that the atom must income at the fixed wavevector $k_L = \frac{\pi}{2}$ through the L channel.

If ξ and ε are specified according to Eqs. (20) and (21), how the atom flows vary with the wavevector k_L for different magnetic flux ϕ can be shown in Fig. 8, where, to guarantee the reality of both k_L and k_R , we have constrained $\arccos(|\varepsilon| - \varepsilon - 2) \leq k_L \leq \arccos(-|\varepsilon| - \varepsilon + 2)$. We can observe that despite the varying of ϕ , the perfect routing always occurs at $k_L = \frac{\pi}{2}$. However, the wavevector k_R for the outgoing atom in the R channel will accordingly change. It is also obvious that the two boundaries of the k_L axis are changed as ϕ varies, which is due to the variation of ε .

V. DISCUSSION AND CONCLUSION

In experiment, the quasimomentum k of the incident ^{87}Rb atoms can be generated via phase imprinting method [28], Bragg scattering, or simply acceleration of the matter-wave probe in an external potential. The localization magnetic flux is achieved by two laser beams whose intersection only covers

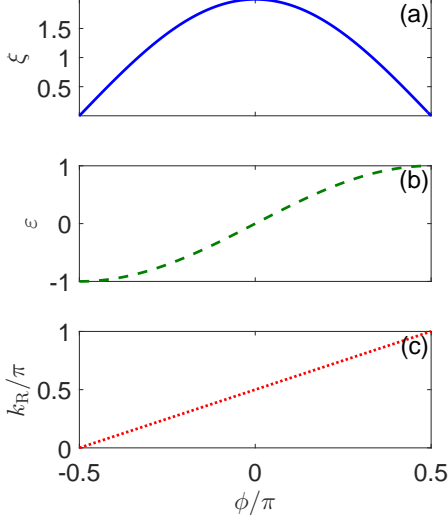


FIG. 7: (color online). (a) Normalized square interleg coupling strength ξ , (b) onsite energy ε , and (c) wave vector k_R in the R channel against the artificial magnetic flux ϕ/π in the condition of perfect routing. Here, we have assumed the intraleg hopping strengths are equal: $J_L = J_R = 1$.

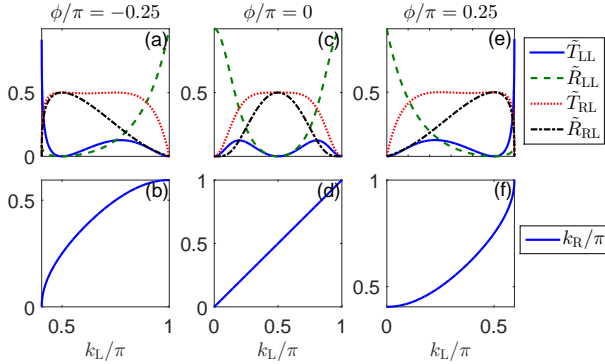


FIG. 8: (color online). Atom flows \tilde{T}_{LL} , \tilde{R}_{LL} , \tilde{T}_{RL} , and \tilde{R}_{RL} , and the corresponding wave vector in the R channel k_R against the wave vector of the incoming atom k_L for the artificial magnetic flux ϕ/π taking (a) and (b) -0.25 , (c) and (d) 0 , and (e) and (f) 0.25 , respectively. In all plots (a)-(f), we have chosen the intraleg hopping strengths $J_L = J_R = 1$ such that the normalized square interleg coupling strength $\xi = K^2$, the interleg hopping strength $K = \sqrt{2} \cos \phi$ such that $\xi = 2 \cos \phi$, and the onsite energy $\varepsilon = J_R \sin \phi$; to guarantee that both k_L and k_R are real, the range of k_L is chosen as $\arccos(|\varepsilon| - \varepsilon - 2) \leq k_L \leq \arccos(-|\varepsilon| - \varepsilon + 2)$.

four lattice sites that encloses the magnetic flux inside the ladder. The interleg hopping strength, magnetic flux, and onsite energy can be tuned via modifying the lasers, e.g., the intensity, angles, and wavevectors. In measurement, the motion of the atoms can be recorded by absorption imaging [29] for furthermore analysis.

In conclusion, we have investigated the single-atom trans-

port in a two leg ladder with only two rungs, which together with the legs, enclose an artificial magnetic flux. Here, the atoms on the two legs possess opposite onsite energies that produce an energy offset. We find that the atom incoming from the left leg can experience from blockade to transparency via modifying the onsite energy, hopping strength, or magnetic flux, which can be potentially used for a quantum switcher. Furthermore, the atom incoming from the left leg can also be perfectly routed into the right leg, when, intriguingly, the outgoing atom in the R channel possesses a wavevector that can be modulated by the magnetic flux. The result may be potentially used for the interface that controls the communication between two individual quantum devices of cold atoms. The method can also be generalized to other artificial quantum systems, such as superconducting quantum circuit system, optomechanical system, etc.

VI. ACKNOWLEDGMENTS

We are grateful to Ru-Quan Wang for helpful discussions. This work is supported by the National Key R&D Program of China under grants No. 2016YFA0301500, NSFC under grants No.s 11847165, 11434015, 61227902, 11611530676, 61775242, 61835013, SPRPCAS under grants No.s XDB01020300, XDB21030300.

Appendix A: Experimental implementation

To create the two-leg ladder model [27], we can apply a standing wave in the y (z) direction with the wave length λ_z (λ_z), but two standing waves in the x direction, which creates a double-well potential: $V_s(x) = V_x \sin^2(k_1 x + \varphi/2) + V_x \sin^2(k_2 x)$ with $k_i = 2\pi/\lambda_i$ and $\lambda_1 = 2\lambda_2$ [see Fig. (9)]. The lattice depths V_x and phase φ are properly chosen to create an array of isolated tilted double well potentials, where each double well realizes a single ladder. In the tight-binding limit, the ladder Hamiltonian can be described by

$$H_{\text{ld}} = \sum_l \frac{\Delta}{2} (b_{l,R}^\dagger b_{l,R} - b_{l,L}^\dagger b_{l,L}) - \sum_{l; q=L,R} J_q b_{l+1,q}^\dagger b_{l,q} - K \sum_l b_{l,L}^\dagger b_{l,R} + \text{H.c.}, \quad (\text{A1})$$

where the tunneling is inhibited by the energy difference Δ , suppose that $\Delta \gg K$ is satisfied.

The generation of the localized artificial magnetic flux is Inspired by Refs. [27, 30, 31, 33]. We control the thickness of both beams such that the intersection of them only cover the very four lattice sites that will enclose the effective magnetic flux [also see Fig. (9)]. We assume two travelling laser beams with wavevectors $\mathbf{k}_i = k_i (\cos \phi_i \mathbf{e}_x + \sin \phi_i \mathbf{e}_y)$ and Rabi frequencies Ω_i ($i = 1, 2$) are employed to illuminate the atoms. Both lasers are incident in the xy -plane at angles ϕ_1 and ϕ_2 , and couple two internal atomic energy levels $|g\rangle$ (ground state) and $|e\rangle$ (intermediate state) through large

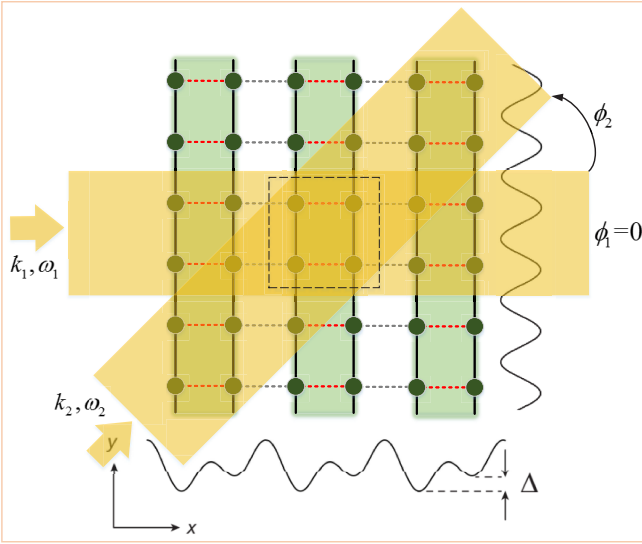


FIG. 9: (color online). Experimental realization of localized effective magnetic fields using two thin Raman lasers. The double-well potential generated in the horizontal direction produce an array of ladders, where the tunneling between adjacent legs is inhibited due to the energy offset Δ . To restore the tunneling, we apply two lasers respectively incoming at the angles ϕ_1 (conveniently, $\phi_1 = 0$ is specified here) and ϕ_2 , whose frequency difference $\omega = \omega_2 - \omega_1$ is nearly resonant with Δ : $\Delta - \omega = -2\varepsilon$ and $|\varepsilon| \ll \Delta$. The tunneling can only be restored at the intersection between the laser beams, where a time-dependent potential [see Eq. (A2)] with frequency ω is induced. Due to the spatial variation of this potential, the resulting hopping term is complex, whose phase factor represents the “magnetic flux” [see the sites inside the dashed rectangle, which encloses an effective magnetic flux ϕ].

detunings δ_i ($|\delta_i| \gg \Omega_i$), which result in an external potential $V_e(\mathbf{r}) = \hbar\Omega \cos[(\mathbf{k}_1 - \mathbf{k}_2)\mathbf{r} + \omega t]$ with $\Omega = \frac{\Omega_1\Omega_2}{2\delta_1}$. Here, the frequency difference ω can be represented by $\omega = c(k_2 - k_1) = \delta_2 - \delta_1$ with $|\omega| \ll |\delta_i|$ such that $\delta_1 \approx \delta_2$. In the tight-binding limit, the external potential corresponds to the Hamiltonian

$$H_e(t) = \hbar\Omega \sum_{l=0,1; q=L,R} \cos(\varphi_{l,q} + \omega t) b_{l,q}^\dagger b_{l,q}, \quad (\text{A2})$$

where $\varphi_{l,L/R} = \mp \frac{k_x \lambda_s}{4} + \frac{l k_y \lambda_s}{2}$. The wavevectors k_x and k_y can be represented as $k_x = k_1 \cos \phi_1 - k_2 \cos \phi_2$ and $k_y = k_1 \sin \phi_1 - k_2 \sin \phi_2$. To eliminate the time-dependent Hamiltonian $H_e(t)$, we perform a unitary transformation $U = \exp[-i \frac{\Omega}{\omega} \sum_{l=0,1; q=L,R} \sin(\varphi_{l,q} + \omega t) b_{l,q}^\dagger b_{l,q}]$, which yields the following effective Hamiltonian

$$\begin{aligned} H_{\text{eff}} = & \sum_l \frac{\Delta}{2} (b_{l,R}^\dagger b_{l,R} - b_{l,L}^\dagger b_{l,L}) \\ & - \sum_{\substack{l \neq -1,0,1 \\ q=L,R}} J_y b_{l+1,q}^\dagger b_{l,q} - \sum_{l \neq 0,1} J_x b_{l,L}^\dagger b_{l,R} + \text{H.c.} \\ & - \sum_{\substack{l=-1,0,1 \\ q=L,R}} J_{l,q} b_{l+1,q}^\dagger b_{l,q} - \sum_{l=0,1} K_l b_{l,L}^\dagger b_{l,R} + \text{H.c.} \end{aligned} \quad (\text{A3})$$

Here, we assume ω is nearly resonant with Δ : $\Delta - \omega = -2\varepsilon$ and $|\varepsilon| \ll \Delta$, which convinces us to discard the fast-oscillating terms. Furthermore, in the perturbative limit ($\frac{\Omega}{\omega} \ll 1$), the parameters take the forms $J_{l,q} \approx J_y$ ($l = -1, 0, \text{ and } 1$), $K_0 \approx K \exp(i\omega t)$, and $K_1 \approx K \exp(i\phi) \exp(i\omega t)$, where the interleg coupling strength $K = \frac{J_x \Omega}{\omega} \cos(\frac{k_x \lambda_s}{4})$, and the effective magnetic flux $\phi = \frac{1}{2} k_y \lambda_s = \frac{1}{2} (k_1 \sin \phi_1 - k_2 \sin \phi_2) \lambda_s$ can be tuned via the Raman lasers, e.g., the angles ϕ_i . Applying the unitary transformation $U' = \exp[-\frac{1}{2} i\omega t \sum_l (b_{l,R}^\dagger b_{l,R} - b_{l,L}^\dagger b_{l,L})]$, we then obtain the Hamiltonian in Eq. (1) as

$$\begin{aligned} H = & \sum_l \varepsilon (b_{l,L}^\dagger b_{l,L} - b_{l,R}^\dagger b_{l,R}) \\ & - \sum_l J_y b_{l+1,L}^\dagger b_{l,L} + J_y b_{l+1,R}^\dagger b_{l,R} + \text{H.c.} \\ & - \sum_{l=0,1} K b_{0,L}^\dagger b_{0,R} + K \exp(i\phi) b_{1,L}^\dagger b_{1,R} + \text{H.c.} \end{aligned} \quad (\text{A4})$$

-
- [1] G. K. Brennen, C. M. Caves, P. S. Jessen, and I. H. Deutsch, Quantum Logic Gates in Optical Lattices, *Phys. Rev. Lett.* **82**, 1060 (1999).
 - [2] D. Jaksch, H. J. Briegel, J. I. Cirac, C. W. Gardiner, and P. Zoller, Entanglement of Atoms via Cold Controlled Collisions, *Phys. Rev. Lett.* **82**, 1975 (1999).
 - [3] J. Pachos and P. L. Knight, Quantum Computation with a One-Dimensional Optical Lattice, *Phys. Rev. Lett.* **91**, 107902 (2003).
 - [4] A. Kay, J. K. Pachos, and C. S. Adams, Graph-State Preparation and Quantum Computation with Global Addressing of Optical Lattices, *Phys. Rev. A* **73**, 22310 (2006).
 - [5] W. Hansel, P. Hommelhoff, T. W. Hansch, and J. Reichel, Bose-Einstein Condensation on a Microelectronic Chip, *Nature* **413**, 498 (2001).
 - [6] J. Fortagh and C. Zimmermann, Toward Atom Chips, *Science* **307**, 860 (2005).
 - [7] Y. Colombe, T. Steinmetz, G. Dubois, F. Linke, D. Hunger, and J. Reichel, Strong Atom-Field Coupling for Bose-Einstein Condensates in an Optical Cavity on a Chip, *Nature* **450**, 272 (2007).
 - [8] M. F. Riedel, P. Bohi, Y. Li, T. W. Hansch, A. Sinatra, and P. Treutlein, Atom-Chip-Based Generation of Entanglement for Quantum Metrology, *Nature* **464**, 1170 (2010).
 - [9] T. van Zoest, N. Gaaloul, Y. Singh, H. Ahlers, W. Herr, S. T. Seidel, W. Ertmer, E. Rasel, M. Eckart, E. Kajari, S. Arnold, G. Nandi, W. P. Schleich, R. Walser, A. Vogel, K. Sengstock, K. Bongs, W. Lewoczko-Adamczyk, M. Schiemangk, T. Schuldt, A. Peters, T. Konemann, H. Muntinga, C. Lammerzahl, H. Dit-tus, T. Steinmetz, T. W. Hansch, and J. Reichel, Bose-Einstein

- Condensation in Microgravity, *Science* **328**, 1540 (2010).
- [10] R. A. Vicencio, J. Brand, and S. Flach, Fano blockade by a bose-einstein condensate in an optical lattice, *Phys. Rev. Lett.* **98**, 184102 (2007).
- [11] Y.-J. Zhao, D. Yu, L. Zhuang, X. Gao, and W.-M. Liu, Tunable Spinful Matter Wave Valve, *Sci. Rep.* **9**, 8653 (2019).
- [12] W.-M. Liu, B. Wu, and Q. Niu, Nonlinear Effects in Interference of Bose-Einstein Condensates, *Phys. Rev. Lett.* **84**, 2294 (2000).
- [13] Z. X. Liang, Z. D. Zhang, and W. M. Liu, Dynamics of a Bright Soliton in Bose-Einstein Condensates with Time-Dependent Atomic Scattering Length in an Expulsive Parabolic Potential, *Phys. Rev. Lett.* **94**, 050402 (2005).
- [14] O. Morsch and M. Oberthaler, Dynamics of Bose-Einstein Condensates in Optical Lattices, *Rev. Mod. Phys.* **78**, 179 (2006).
- [15] A. E. Miroshnichenko, S. Flach, and Y. S. Kivshar, Fano Resonances in Nanoscale Structures, *Rev. Mod. Phys.* **82**, 2257 (2010).
- [16] Y. V. Kartashov, B. A. Malomed, and L. Torner, Solitons in Nonlinear Lattices, *Rev. Mod. Phys.* **83**, 247 (2011).
- [17] C.-C. Chien, S. Peotta, and M. Di Ventra, Quantum Transport in Ultracold Atoms, *Nat. Phys.* **11**, 998 (2015).
- [18] U. V. Poulsen and K. Mølmer, Scattering of Atoms on a Bose-Einstein Condensate, *Phys. Rev. A* **67**, 013610 (2003).
- [19] A. Smerzi and A. Trombettoni, Nonlinear Tight-Binding Approximation for Bose-Einstein Condensates in a Lattice, *Phys. Rev. A* **68**, 023613 (2003).
- [20] C. X. Zhang, B. Zhou, Y. H. Nie, J. Q. Liang, and J. Liu, Scattering Effect of Atoms through a Bose-Einstein Condensate in an Optical Lattice with a Single Defect, *Eur. Phys. J. D* **49**, 161 (2008).
- [21] E. Arévalo, Solitary Wave Solutions as a Signature of the Instability in the Discrete Nonlinear Schrödinger Equation, *Phys. Lett. A* **373**, 3541 (2009).
- [22] H. Hennig, J. Dornigac, and D. K. Campbell, Transfer of Bose-Einstein Condensates through Discrete Breathers in an Optical Lattice, *Phys. Rev. A* **82**, 053604 (2010).
- [23] X.-D. Bai, Q. Ai, M. Zhang, J. Xiong, G.-J. Yang, and F.-G. Deng, Stability and Phase Transition of Localized Modes in Bose-Einstein Condensates with Both Two- and Three-Body Interactions, *Ann. Phys.* **360**, 679 (2015).
- [24] X. D. Bai, B. A. Malomed, and F. G. Deng, Unidirectional Transport of Wave Packets through Tilted Discrete Breathers in Nonlinear Lattices with Asymmetric Defects, *Phys. Rev. E* **94**, 032216 (2016).
- [25] R. Qi, X.-L. Yu, Z. B. Li, and W. M. Liu, Non-Abelian Josephson Effect between Two $f = 2$ Spinor Bose-Einstein Condensates in Double Optical Traps, *Phys. Rev. Lett.* **102**, 185301 (2009).
- [26] L. Zhou, L.-P. Yang, Y. Li, and C. P. Sun, Quantum Routing of Single Photons with a Cyclic Three-Level System, *Phys. Rev. Lett.* **111**, 103604 (2013).
- [27] M. Atala, M. Aidelsburger, M. Lohse, J. T. Barreiro, B. Paredes, and I. Bloch, Observation of Chiral Currents with Ultracold Atoms in Bosonic Ladders, *Nat. Phys.* **10**, 588 (2014).
- [28] J. Denschlag, J. E. Simsarian, D. L. Feder, C. W. Clark, L. A. Collins, J. Cubizolles, L. Deng, E. W. Hagley, K. Helmerston, W. P. Reinhardt, S. L. Rolston, B. I. Schneider, and W. D. Phillips, Generating Solitons by Phase Engineering of a Bose-Einstein Condensate, *Science* **287**, 97 (2000).
- [29] Y. Lin, K. Jimenezgarcia, and I. B. Spielman, Spin-Orbit-Coupled Bose-Einstein Condensates, *Nature* **471**, 83 (2011).
- [30] M. Aidelsburger, M. Atala, S. Nascimbène, S. Trotzky, Y. A. Chen, and I. Bloch, Experimental Realization of Strong Effective Magnetic Fields in an Optical Lattice, *Phys. Rev. Lett.* **107**, 255301 (2011).
- [31] M. Aidelsburger, M. Atala, M. Lohse, J. T. Barreiro, B. Paredes, and I. Bloch, Realization of the Hofstadter Hamiltonian with Ultracold Atoms in Optical Lattices, *Phys. Rev. Lett.* **111**, 185301 (2013).
- [32] H. Miyake, G. A. Siviloglou, C. J. Kennedy, W. C. Burton, and W. Ketterle, Realizing the Harper Hamiltonian with Laser-Assisted Tunneling in Optical Lattices, *Phys. Rev. Lett.* **111**, 185302 (2013).
- [33] D. Jaksch and P. Zoller, Creation of Effective Magnetic Fields in Optical Lattices: The Hofstadter Butterfly for Cold Neutral Atoms, *New J. Phys.* **5**, 56 (2003).